Building Research & Information (2008) 36(2), 111–128

Impact of climate warming on passive night cooling potential

N. Artmann[1], D. Gyalistras[2], H. Manz[1] and P. Heiselberg[3]

[1]Empa, Swiss Federal Laboratories for Materials Testing and Research, Laboratory for Building Technologies, CH-8600 Duebendorf, Switzerland
E-mails: nikolai.artmann@empa.ch and heinrich.manz@empa.ch

[2]Institute for Integrative Biology, ETH Zurich, CH-8092 Zurich, Switzerland
E-mail: gyalistras@env.ethz.ch

[3]Hybrid Ventilation Centre, Department of Civil Engineering, Aalborg University, DK-9000 Aalborg, Denmark
E-mail: ph@civil.aau.dk

Night-time ventilation is often seen as a promising passive cooling concept. However, as it requires a sufficiently high temperature difference between ambient air and the building structure, this technique is highly sensitive to changes in climatic conditions. In order to quantify the impact of climate warming on the night-time ventilative cooling potential in Europe, eight representative locations across a latitudinal transect were considered. Based on a degree-hours method, site-specific regression models were developed to predict the climatic cooling potential (CCP) from minimum daily air temperature (T_{min}). CCP was computed for present conditions (1961–90) using measured T_{min} data from the European Climate Assessment (ECA) database. Possible time-dependent changes in CCP were assessed for 1990–2100, with particular emphasis on the Intergovernmental Panel on Climate Change (IPCC) 'A2' and 'B2' scenarios for future emissions of greenhouse gases and aerosols. Time-dependent, site-specific T_{min} scenarios were constructed from 30 Regional Climate Model (RCM) simulated data sets, as obtained from the European PRUDENCE project. Under both emissions scenarios and across all locations and seasons, CCP was found to decrease substantially by the end of the 21st century. For the six Central and Northern European locations (>47°N) CCP was found to decrease in summer (June–August) by 20–50%. For the two Southern European locations (Madrid and Athens), future CCP was found to become negligible during the summer and to decrease by 20–55% during the spring and the autumn. The study clearly shows that night-time cooling potential will cease to be sufficient to ensure thermal comfort in many Southern and Central European buildings. In Central and Northern Europe, a significant passive cooling potential is likely to remain, at least for the next few decades. Upper and lower bound estimates for future CCP were found to diverge strongly in the course of the 21st century, suggesting the need for flexible building design and for risk assessments that account for a wide range of emissions scenarios and uncertainty in climate model results.

Keywords: climate change, climate scenarios, climatic cooling potential, night-time ventilation, passive cooling, Europe

La ventilation nocturne est souvent considérée comme un concept de refroidissement passif prometteur. Toutefois, cette technique nécessitant une différence de température suffisamment élevée entre l'air ambiant et la structure du bâtiment, elle est très sensible aux changements des conditions climatiques. Pour quantifier l'impact du réchauffement climatique sur les possibilités de refroidissement par ventilation nocturne, on a considéré huit emplacements représentatifs sur une transversale latitudinale en Europe. Sur la base d'une méthode 'degrés-heures', on a développé des modèles de régression spécifiques à des sites pour prévoir le potentiel de refroidissement climatique (CCP) à partir de la température quotidienne minimale de l'air (T_{min}). On a calculé le CCP pour les conditions présentes pendant la période 1961–90

Building Research & Information ISSN 0961-3218 print/ISSN 1466-4321 online © 2008 Taylor & Francis
http://www.tandf.co.uk/journals
DOI: 10.1080/09613210701621919

en utilisant les données T_{min} de la base de données ECA (Evaluation du climat européen). On a évalué de possibles changements du CCP liés à la durée pour la période 1990–2100, en mettant l'accent sur les scénarios A2 et B2 du GIEC (Groupe d'experts intergouvernemental sur l'évolution du climat) relatifs aux futures émissions de gaz à effet de serre et aux aérosols. Des scénarios liés à la durée, avec T_{min} spécifiques aux sites ont été élaborés à partir de 30 ensembles de données de modèles de climats régionaux simulés obtenus dans le cadre du projet européen PRUDENCE. Pour les deux scénarios d'émission et pour tous les emplacements et saisons, on a constaté que le CCP diminuait de façon substantielle dès la fin du XXIe siècle. Pour les six emplacements en Europe centrale et en Europe du Nord (>47° nord), on a constaté que le CCP diminuait de 20–50% (juin–août). Pour les deux emplacements en Europe du Sud (Madrid et Athènes), on a constaté que le futur CCP devenait négligeable pendant l'été et diminuait de 20–55% pendant le printemps et l'automne. Cette étude montre clairement que le potentiel de refroidissement nocturne cessera d'être suffisant pour assurer le confort thermique dans de nombreux bâtiments construits en Europe du Sud et en Europe centrale. En Europe centrale et en Europe du Nord, un potentiel significatif de refroidissement passif va vraisemblablement durer pendant au moins les prochaines décennies. Il s'est avéré que les estimations supérieures et inférieures du futur CCP divergeaient nettement dans le courant du XXIe siècle, ce qui suggère la nécessité de concevoir les bâtiments avec souplesse et d'évaluer le risque en tenant compte d'une large gamme de scénarios d'émission et de l'incertitude des résultats des modèles climatiques.

Mots clés: changements climatiques, scénarios climatiques, potentiel de refroidissement climatique, ventilation nocturne, refroidissement passif, Europe

Introduction

As a consequence of increasing atmospheric concentrations of greenhouse gases, significant changes in the global climate are expected. The globally and annually averaged near-surface temperature has been estimated to have increased by 0.74 ± 0.18°C over the last century (1906–2005), with the rate of warming over the last 50 years being almost double that over the last century (Trenberth *et al.*, 2007). Applying six different marker scenarios for possible future emissions of radiatively active gases and aerosols, projections from a range of climate models suggest by the end of the 21st century a warming rise of 1.1–6.4°C will occur as compared with 1980–99 (Meehl *et al.*, 2007). This warming trend will be accompanied by complex and significant changes in regional climates that nowadays can be studied in increasing spatio-temporal detail with the aid of regional climate models (Giorgi *et al.*, 2001).

Climate change will impact in a variety of ways on the built environment and buildings (Engineering and Physical Sciences Research Council (EPSRC), 2003; Chartered Institution of Building Services Engineers (CIBSE), 2005). In particular, rising ambient temperatures imply a decrease in heating energy demand for buildings, but also an increasing demand for cooling. For Switzerland, for example, recent studies employing a degree-days method (Christenson *et al.*, 2005) and transient building energy simulations (Frank, 2005) demonstrated significant 20th-century trends in building energy demand that are likely to continue throughout the 21st century due to ongoing climate warming.

Even for the colder climate of the UK an increased risk of summertime overheating is expected as the occurrence of times with temperatures over 28°C was found to rise from 1 to 6% by the 2080s. Simulation studies revealed the application of thermal mass for building cooling to be very helpful, but due to a more frequent occurrence of hot spells, an effective way to dissipate the heat from the mass is seen to be essential (CIBSE, 2005).

Not only climate change, but also increased comfort expectations in summertime, high internal loads, and, especially in modern, extensively glazed buildings, higher solar gains (Manz, 2004; Manz and Frank, 2005) contribute to an increasing demand for cooling of buildings. Thus, commercial buildings in particular have experienced an upward trend in cooling energy demand over the last few decades, and the installation of air-conditioning systems is becoming more common even in the moderate and cool climates of Central and Northern Europe.

Particularly in this case – commercial buildings with high cooling loads in moderate climates with relatively low night-time temperatures even in summer – passive cooling by night-time ventilation appears to offer considerable potential. The basic concept involves cooling the building structure overnight in order to provide a heat sink, which absorbs heat gains during occupancy periods, and to guarantee thermal comfort without mechanical cooling or, at least, with a lower daytime cooling energy requirement (Chandra, 1989; Santamouris and Asimakopoulos, 1996; Allard, 1998). Night-time ventilation can be driven by natural forces (thermal buoyancy and wind), mechanical fans or hybrid ventilation systems. However, as in any case a sufficiently large temperature difference between ambient air and the building structure is needed during the night to achieve efficient convective cooling

of the building mass; this concept is highly dependent on climatic conditions and its potential could be jeopardized by climate warming.

For current European climatic conditions, the potential of passive cooling by night-time ventilation was investigated using a degree-hours method (Artmann *et al.*, 2007). The potential was found to be very significant in Northern Europe (including the British Isles), and still sufficient on most nights of the year in Central and Eastern Europe. In Southern Europe passive night-time cooling might not be sufficient the whole year round, but could still be used in hybrid systems.

Eicker *et al.* (2006) provided experimental evidence for the limitations of night-time ventilation under climatic conditions currently regarded as extreme. They monitored for three years an advanced low-energy office building in Weilheim, Germany, which was constructed in 1999, that was also equipped with an earth-to-air heat exchanger. While the building performed excellently during typical German summer conditions (2001 and 2002), in 2003, with average summer temperatures more than 3 K higher than usual, nearly 10% of all office hours were above 26°C. As the temperatures observed during the exceptionally hot summer of 2003 might correspond to those of a typical summer at the end of this century (Schaer *et al.*, 2004), the findings of Eicker *et al.* clearly demonstrate that in decades to come cooling by night-time ventilation might cease to work in buildings designed for current climatic conditions.

The impact of climate change on different passive cooling techniques has been analysed by Roaf *et al.* (1998). For the applicability of night-time ventilation, a monthly mean daily maximum temperature of 31°C was assumed to be the limiting criterion. Based on this and other threshold values, they delineated the regions where different cooling techniques could cease to be viable by 2050. These were found to be extensive enough to make them conclude that the effects of global warming should be taken into account by designers.

However, the study of Roaf *et al.* (1998) suffers from several shortcomings. First, their threshold temperature of 31°C only applies to well-shaded buildings with relatively low internal loads (e.g. residential buildings), as the authors state. Second, their threshold-based method is not suitable for quantifying gradual changes in cooling potential, e.g. across spatial gradients or over time. Although their approach was suitable to detect first-order effects, the 'cascade of uncertainty' associated with any regional climate projections (Gyalistras *et al.*, 1998; Mearns *et al.*, 2001) should also be taken into account for the elaboration of guidelines.

Uncertainty in climate projections arises, first of all, from the basic unpredictability of the socio-economic system and technological development. This makes it necessary to formulate a wide range of scenarios for the future emission of radiatively active gases and aerosols (Nakicenovic *et al.*, 2000). Further uncertainties are added in the process of estimating concentrations from emissions, radiative forcing from concentrations, and global climate changes from forcing. The most sophisticated tools available to accomplish the last step are what are known as Atmosphere–Ocean General Circulation Models (AOGCM) – global models with a rather coarse horizontal resolution of 200–300 km (Cubasch *et al.*, 2001). AOGCM results can be used as initial and boundary conditions for Regional Climate Models (RCM), to simulate local climatic effects for smaller areas, e.g. Europe, on a finer grid of about 50 km (Christensen *et al.*, 2002). This last 'downscaling' step again introduces additional uncertainty related to limitations of the available data, knowledge and AOGCMs/RCMs.

Nonetheless, it is assumed in this work that careful analysis of a wider range of regional climate scenarios can be used to provide upper and lower limits on the future space–time evolution of the cooling potential by night-time ventilation. Specifically, in this study the implications of two selected global emissions scenarios on cooling potential across eight representative sites in Europe are explored. This is accomplished by combining the degree-hours method of Artmann *et al.* (2007) with state-of-the-art temperature scenarios for 2071–2100, as derived from simulations with 12 RCMs driven by six different AOGCMs. The significant impact of climate warming on the potential for cooling by night-time ventilation is assessed, uncertainties associated with the applied scenarios and method are quantified, and consequences for building design are discussed.

Materials and methods

Case study locations

In the wake of inherent stochastic weather patterns, the potential for night-time cooling is subject to wide fluctuation in space and time (Artmann *et al.*, 2007). Moreover, it depends non-linearly on meteorological conditions, and this makes the use of coarse weather data (e.g. averages over a month or larger regions) problematic. Therefore, in this study representative locations were chosen for a more detailed analysis using hourly and daily weather data. The considered locations represent different climatic zones across a North–South transect in Europe (Table 1 and Figure 1). Table 1 also includes daily minimum temperature statistics based on long-term measurement data (1961–90) provided by the European Climate Assessment (ECA).

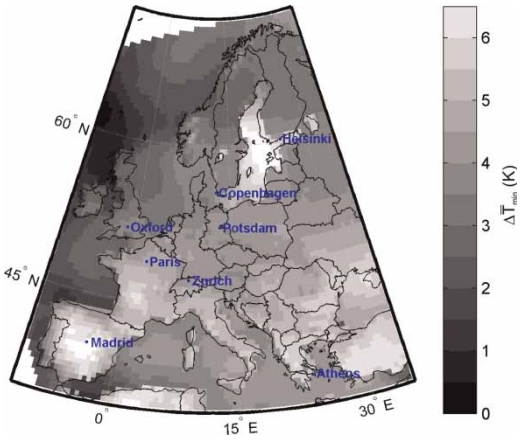

Figure 1 Change in long-term mean daily minimum temperature, $\Delta\overline{T}$, in summer (June–August) over Europe under the 'A2' emissions scenario for 2071–2100 relative to the baseline 1961–90, as simulated by the Danish Meteorological Institute regional climate model. Simulations were based on boundary conditions from the HadAM3H atmospheric general circulation model (Table A1, scenario No S1). Data are from PRUDENCE (2006)

Observed weather and climate data

Two sources of observed weather and climate data were used. The first was the commercial Meteonorm (2005) database that contains measurements from 7400 stations around the world. The database comes with software to generate semi-synthetic hourly weather data from measured long-term monthly mean values of weather variables (mainly representative of the period 1961–90) by means of stochastic simulation. Data for all case study locations were available in the Meteonorm database. Five different sets of random numbers were used at each location to generate a one-year data set of hourly mean temperature. The resulting sample size was 5×365 days $\times$ 24 hours. The applicability of these data for the calculation of the climatic cooling potential has been shown previously (Artmann *et al.*, 2007).

The second source of measured weather data was daily minimum temperatures (T_{min}) for 1961–90 as provided by the ECA (Klein Tank *et al.*, 2002). For easier handling the data sets were reduced to 360 days per year. This was accomplished by excluding all values for 29 February and 31 March, May, July, August and October. This procedure yielded 90 values per season. Winter was defined as December–February, spring as March–May, summer as June–August, and autumn as September–November. The resulting sample size for the 30-year period was 2700 daily values per season.

Model-simulated temperature data

All calculations of climate change effects were based on changes in the seasonal statistics of daily minimum temperatures (T_{min}) as simulated by a range of state-of-the-art RCMs. All RCM data were obtained from the PRUDENCE project (Christensen *et al.*, 2002, 2007; PRUDENCE, 2005). This project represented an attempt to integrate European climate projections of different institutions, and its website (PRUDENCE, 2006) provides a large database of RCM simulation results for Europe. These were based on boundary conditions from six global simulations with two AOGCMs (Arpege/OPA and ECHAM4/OPYC), plus three atmosphere-only GCMs (ECHAM5, HadAM3H and HadAM3P) that were driven with sea-surface temperature and sea-ice boundary conditions taken from simulations with the HadCM3 AOGCM. More information about the climate simulation models can be found on the PRUDENCE website.

Two kinds of RCM-simulated T_{min} data were used: 'control' data from regional climate RCM simulations under present-day (1961–90) conditions, and 'scenario' data for 2071–2100 under the emissions scenarios 'A2' and 'B2', as described in the Intergovernmental Panel on Climate Change's (IPCC) Special Report on Emission Scenarios (SRES) (Nakicenovic *et al.*, 2000; Intergovernmental Panel on Climate Change (IPCC), 2006).

All T_{min} data available from the PRUDENCE website, in total 20 control and 30 scenario runs, were initially considered (Table A1). This yielded a total of $n_{Ctrl} = 636$ and $n_{Scen} = 956$ seasonal data sets (=20 or 30 $\times$ eight locations $\times$ four seasons, minus four cases with no RCM data available for Madrid).

The RCM data were provided on varying model grids. For all calculations in this study the near-surface temperature data from the land gridpoint closest to the respective case study location were used for each RCM.

RCM control climates may deviate substantially from observations due to errors in the driving GCMs and to RCM deficiencies or omissions regarding the representation of the topography (e.g. inland bodies of water, mountains), and relevant processes (such as sea-ice or vegetation dynamics). In order to exclude 'unrealistic' RCM data sets the control data from all RCMs were first compared with the corresponding ECA measurements. To account for regional and seasonal variation in model performance for each selected grid point and season the 30-year long-term means ($\overline{T}_{min}$) and standard deviations (S) of the measured (subscript 'Obs' in the following equations; S in Table 1) and under present-day conditions simulated (subscript Ctrl) T_{min} data were computed. The simulated $\overline{T}_{min}$ were then corrected for the difference in altitude between the RCM grid point (H_{RCM}) and the

Table 1 Geographical position and altitude of the considered locations

Location	Longitude (°:')	Latitude (°:')	Altitude (masl)	Season	$\overline{T}_{min}$(°C)	S (°C)[1]	S_{sm} (°C)[2]
Helsinki	24:57 E	60:10 N	4	December–February	−7.55	7.21	3.20
				March–May	0.29	6.10	1.39
				June–August	12.39	3.00	0.93
				September–November	3.82	5.66	1.25
Copenhagen	12:32 E	55:41 N	9	December–February	−0.92	3.92	2.01
				March–May	3.83	4.30	0.95
				June–August	12.90	2.49	0.65
				September–November	7.21	4.15	0.69
Potsdam	13:04 E	52:23 N	81	December–February	−2.66	5.24	2.40
				March–May	3.75	4.87	0.97
				June–August	12.42	2.94	0.55
				September–November	5.78	4.80	0.76
Oxford	1:16 W	51:46 N	63	December–February	1.75	4.08	1.55
				March–May	4.87	3.53	0.58
				June–August	11.69	2.66	0.60
				September–November	7.32	4.34	0.73
Paris	2:20 E	48:49 N	75	December–February	2.50	4.19	1.52
				March–May	7.08	3.89	0.74
				June–August	14.41	2.79	0.81
				September–November	9.06	4.36	0.64
Zurich	8:34 E	47:23 N	556	December–February	−1.83	4.24	1.68
				March–May	4.25	4.42	0.89
				June–August	12.34	2.89	0.61
				September–November	6.25	4.76	0.81
Madrid	3:39 W	40:25 N	667	December–February	3.13	3.06	1.15
				March–May	7.63	3.74	0.89
				June–August	16.87	3.11	0.94
				September–November	10.42	4.86	0.95
Athens	23:45 E	37:54 N	15	December–February	7.75	3.42	0.81
				March–May	11.97	3.91	0.84
				June–August	21.82	2.52	0.86
				September–November	15.74	4.22	0.75

Notes: Data are long-term mean values, $\overline{T}_{min}$; the standard deviation of daily values, S; and the standard deviation of seasonal mean values, S_{sm}, of the daily minimum temperature for winter (December–February), spring (March–May), summer (June–August) and autumn (September–November) (ECA data, 1961–90).

[1] S is defined as follows:

$$S = \left(\frac{1}{2700 - 1} \sum_{y=1961}^{1990} \sum_{d=1}^{90} (T_{\min,y,s,d} - \overline{T}_{\min,s})^2 \right)^{1/2}$$

[2] S_{sm} is defined as follows:

$$S_{sm} = \left(\frac{1}{30 - 1} \sum_{y=1961}^{1990} (\overline{T}_{\min,y,s} - \overline{T}_{\min,s})^2 \right)^{1/2}$$

measurement station (H_{Obs}) using a standard atmosphere temperature lapse rate:

$$\gamma = -0.0065\,\mathrm{K/m}.$$

The following error measures were considered:

$$\delta\overline{T} = \overline{T}_{\min,Ctrl} + \gamma(H_{RCM} - H_{Obs}) - \overline{T}_{\min,Obs} \quad (1)$$

$$\delta S = \frac{S_{Ctrl}}{S_{Obs}}. \quad (2)$$

Formal statistical testing of the above differences did not prove to be very helpful due to the very large sample sizes of the data sets compared ($n = 2700$). As a consequence, even very small deviations that were neither physically meaningful nor relevant for the present application proved to be highly significant. Therefore, the following criteria were considered instead: data from an RCM for a given season and location were only used if $|\delta\overline{T}| \leq 2K$ and $|\delta S - 1| \leq 20\%$.

The choice of the above threshold values was based on the consideration of the climate change 'signals'. These

were defined as follows:

$$\Delta\overline{T} = \overline{T}_{\mathrm{min,Scen}} - \overline{T}_{\mathrm{min,Ctrl}} \quad (3)$$

$$\Delta S = \frac{S_{\mathrm{Scen}}}{S_{\mathrm{Ctrl}}}, \quad (4)$$

where the subscript 'Scen' denotes a statistic derived from an RCM scenario data set. The control and scenario run pairs used are shown in Table A1.

The threshold value of 2 K for model selection was chosen based on the assumption that in order to be able to 'trust' a given scenario, the model error $\delta\overline{T}$ should be smaller than the signal $\Delta\overline{T}$. In 95% of the n_{Scen} cases considered $\Delta\overline{T}$ was larger than +2 K

In contrast to the changes in the mean, which always increased, the standard deviation decreased or increased depending on seasons and locations, with 90% of all ΔS values falling within the range 0.79–1.26. The threshold value of 20% used for model selection corresponded to the requirement that model errors for S should not be larger than the changes 'typically' simulated for this statistic.

Figure 1 shows by way of example the $\Delta\overline{T}$ signal for summer as modelled by the RCM of the Danish Meteorological Institute (DMI) based on driving data from an A2 scenario integration with the HadAM3H AOGCM (Table A1: Scenario S1). The trend is particularly marked in Southern Europe, totalling 5.0–6.5 K for Central Spain. A similarly pronounced shift emerges in the Baltic Sea region. In Northern, Central and Eastern Europe too the shift in summer mean daily minimum temperature simulated by this model still reaches 2.5–5.0 K. Similarly, complex change patterns were also found for the other scenario simulations and seasons.

Construction of temperature scenarios

Two types of scenarios for possible changes in T_{min} were considered: (1) scenarios describing possible future distributions of T_{min} for 2071–2100 ('static scenarios'); and (2) scenarios describing possible time-dependent changes in the distribution of T_{min} for 1990–2100 ('transient scenarios'). The following procedures were applied separately for each RCM scenario data set, season and location.

For the static scenarios future ('projected', subscript 'Proj') temperature values for all days ($1 \le d \le 2700$) of a given season, $T_{\mathrm{min,Proj}(d)}$, were constructed by adjusting the mean and standard deviation of the measured ECA data according to the respective climate change signals:

$$T_{\mathrm{min,Proj}(d)} = \overline{T}_{\mathrm{min,Obs}} + (T_{\mathrm{min,Obs}(d)} - \overline{T}_{\mathrm{min,Obs}}) \cdot \Delta S + \Delta\overline{T}. \quad (5)$$

The construction of transient scenarios was based on the assumption that the climate change signals $\Delta\overline{T}$ and ΔS for a given future time-point to a first approximation scale linearly with the change in the expected value of the globally and annually averaged near-surface temperature, $\Delta\overline{T}_g$, for that time-point ('pattern scaling' technique; e.g. Mitchell, 2003). Daily data for a given future time point ($1990 \le t \le 2100$) were thus constructed according to:

$$T_{\mathrm{min,Proj}(t,d)} = \overline{T}_{\mathrm{min,Obs}} + (T_{\mathrm{min,Obs}(d)} - \overline{T}_{\mathrm{min,Obs}}) \cdot (1 + \kappa \cdot \Delta\overline{T}_{g(t)}) + \lambda \cdot \Delta\overline{T}_{g(t)} \quad (6)$$

The coefficients $\kappa = \partial\Delta S/\partial\overline{T}_g$ and $\lambda = \partial\Delta\overline{T}/\partial\overline{T}_g$ were estimated separately for each RCM, season and location as follows:

$$\kappa = \left(\frac{S^*_{\mathrm{Scen}}}{S_{\mathrm{Ctrl}}} - 1\right)/\Delta\overline{T}_{\mathrm{GCM}} \quad (7)$$

$$\lambda = \Delta\overline{T}/\Delta\overline{T}_{\mathrm{GCM}}, \quad (8)$$

where S^*_{Scen} is the standard deviation of the linearly detrended (see below) T_{min} scenario data; and $\Delta\overline{T}_{\mathrm{GCM}}$ is the 2071–2100 mean value of ΔT_g, as simulated by the (AO-)GCM used to drive the respective RCM scenario run. Only models with available values of $\Delta\overline{T}_{\mathrm{GCM}}$ (Table A1) were considered for the construction of transient scenarios.

The need to use S^*_{Scen} instead of S_{Scen} arose from the fact that T_{min} showed an upward trend in the 2071–2100 period due to ongoing climate change in the driving GCMs. This trend was considered as an integral part of the static scenarios used to describe the climate of the entire 2071–2100 period. The situation was different with regard to the transient scenarios, since these aimed at describing the statistics of T_{min} for distinct time points. Using non-detrended data would have inflated the standard deviation estimate for the period's central time point ($t = 2085$), thus also leading to a systematic overestimation of κ.

Detrending was performed as follows: first, seasonal means of T_{min} were computed for each year in the 2071–2100 period. The trend was then estimated as the slope of the linear regression of the 30 seasonal means from the year number. Finally, each daily value for a given year was adjusted by subtracting the linear trend component of the corresponding year. S^*_{Scen} was found to be always smaller than S_{Scen}, in

10% of all n_{scen} cases the difference amounted to more than 2% (a maximum of 8%).

For $\Delta\overline{T}_g$ an 'upper' and a 'lower' scenario as provided by Cubasch *et al.* (2001, figure 9.14, 'several models, all SRES envelope') were considered. These $\Delta\overline{T}_g$ trajectories accounted for a much broader range of radiative forcing scenarios and possible $\Delta\overline{T}_g$ responses to a given forcing (climate sensitivities) than was represented in the original PRUDENCE scenarios. The $\Delta\overline{T}_g$ for 2090–99 relative to 1980–99 for the 'upper' ('lower') scenario was 1.3°C (5.5°C). However, it should be noted that these upper and lower bounds still did not account for the full range of possible future developments (Cubasch *et al.*, 2001).

Transient scenarios were constructed by evaluating the $\Delta\overline{T}_g$ data at every five years within the period 1990–2100, and by using the κ and λ values derived from all selected RCM simulations for a given season and location.

Definition of the 'climatic cooling potential'

The potential for passive cooling of buildings by night-time ventilation was assessed based on a degree-hour method that evaluates the difference between the building and the ambient temperature. The method has been presented, extensively tested, and used to assess present-day cooling potentials (Artmann *et al.*, 2007). Therefore, it is described only very briefly here.

The method requires temperature data at an hourly time step as an input and gives the climatic cooling potential in degree hours (Kh). The daily climatic potential for ventilative night cooling, $CCP_{(d)}$, is defined as a summation of products between building/external air temperature difference, $T_b - T_e$ and time interval, m:

$$CCP_{(d)} = \sum_{h=h_i}^{h_f} m_{(d,h)}(T_{b(d,h)} - T_{e(d,h)}) \qquad (9)$$

$$\begin{cases} m = 1\,\text{h} & \text{if} \quad T_b - T_e \geq \Delta T_{crit} \\ m = 0 & \text{if} \quad T_b - T_e < \Delta T_{crit} \end{cases}$$

where d is the day; h is the time of day, where $h \in \{0, \ldots, 23\}$, h_i; h_f is the initial and final time of night-time ventilation; and ΔT_{crit} is a threshold value specifying a minimum temperature difference that is required for effective convection. Throughout all calculations $h_i = 19$, $h_f = 7$ and $\Delta T_{crit} = 3$K were assumed.

Because heat gains and night-time ventilation typically do not coincide in time, energy storage is an inherent part of the passive cooling concept. As building structures are almost always made of materials which are suitable for sensible energy storage only, such as concrete or brick, the temperature of the building structure varies when energy is stored or released. To take this fact into account, a variable building temperature was used for the calculation of the climatic cooling potential. In order to obtain a model which is as general as possible, no building-specific parameters were employed. Instead, the building temperature, T_b, was assumed to oscillate harmonically:

$$T_{b(d,h)} = 24.5°\text{C} + 2.5°\text{C}\cos\left(2\pi\frac{h - h_i}{24}\right)\forall d. \qquad (10)$$

According to this simple model, the maximum building temperature occurs at the initial time of night-ventilation, h_i, and as the ventilation time is 12 hours, the minimum building temperature occurs at the final time, h_f (Figure 2). In real buildings, depending on the direction of the building facade and the ratio of internal and solar gains, the maximum building temperature typically occurs between 14.00 hours ($h = 14$) and 18.00 hours ($h = 18$). Especially for high thermal mass buildings with high internal gains, a shift of the maximum to later hours is typical.

The choice of the building temperature range was based on CEN report CR 1752 (1998), which distinguishes three different categories of summertime thermal comfort, each based on a mean temperature of 24.5°C: category A ±1.0°C, category B ±1.5°C, category C ±2.5°C. International standard ISO 7730 (International Standards Organization (ISO), 1994) also recommends a temperature range of $T = 24.5 \pm 1.5$°C as summer conditions. However, recent studies confirm that broader temperature ranges are acceptable in non-air-conditioned buildings (Olesen and Parsons, 2002).

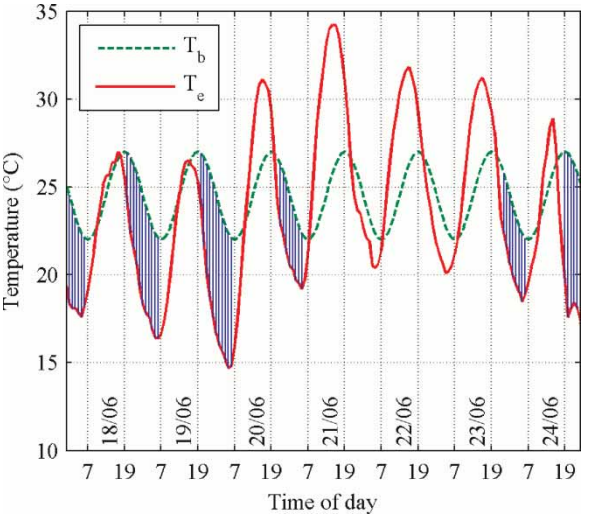

Figure 2 Building temperature, T_b, and external air temperature, T_e, during one week in summer 2003 for Zurich SMA (ANETZ data). Shaded areas illustrate the Climatic Cooling Potential (after Artmann *et al.*, 2007)

Category C of CR 1752 was therefore employed, i.e. $T_b = 24.5 \pm 2.5$°C was assumed for all calculations.

An example of the practical significance of the defined potential showed that a *CCP* of about 80 Kh per night is needed to discharge heat gains of 50 W/m^2 during 8 h using a ventilation rate of 6 air changes per hour (ACH) (Artmann *et al.*, 2007). However, as building parameters as well as heat gains can vary significantly, this value should be seen as a rough indication only.

In this study the following were considered for each season and location: (1) the distribution of $CCP_{(d)}$ and (2) the long-term mean values:

$$\overline{CCP} = \frac{1}{N}\sum_{d=1}^{N} CCP_{(d)}, \qquad (11)$$

where $N = 2700$.

Estimation of the 'climatic cooling potential' from daily minimum temperature

Because no hourly temperature data were available from the PRUDENCE simulations, $CCP_{(d)}$ had to be estimated from daily minimum temperatures, $T_{\min(d)}$. This was done based on the following equation:

$$CCP_{(d)} = \begin{cases} (T_0 - T_{\min(d)} \cdot \mathrm{C} & \text{if } T_{\min(d)} < T_0 \\ 0 & \text{if } T_{\min(d)} \geq T_0 \end{cases} \qquad (12)$$

The threshold temperatures, T_0, and the coefficients, C, were determined separately for each location by linearly regressing the $CCP_{(d)}$ values as calculated from hourly Meteonorm data (equations 9 and 10) with the corresponding $T_{\min(d)}$ data, i.e. the minima of the 24-hourly values per day. T_0 was defined as the temperature at which the regression line intersects the x-axis.

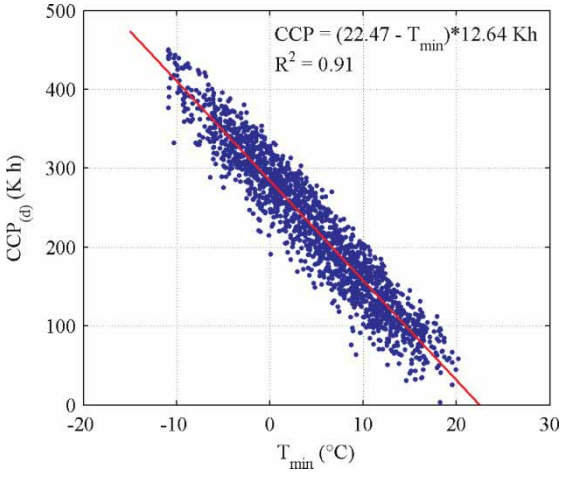

Figure 3 Correlation between daily climatic cooling potential ($CCP_{(d)}$) and daily minimum temperature (T_{min}) based on Meteonorm data for location Zurich SMA

Table 2 Threshold temperatures, T_0, and coefficients, C, for the eight case study locations

Location	T_0 (°C)	C (Kh/K)	R^2
Helsinki	24.11	12.17	0.91
Copenhagen	22.87	12.31	0.88
Potsdam	22.20	12.21	0.85
Oxford	24.07	11.23	0.78
Paris	22.25	12.22	0.83
Zurich	22.47	12.64	0.91
Madrid	19.67	12.92	0.87
Athens	21.86	12.82	0.89

An example for the location Zurich SMA is given in Figure 3. The results for all locations are summarized in Table 2.

Results

Figure 4 shows the seasonal $\overline{CCP}$ values found at the eight locations (arranged from left to right by latitude) under present-day (1961–90) and possible future conditions (2071–2100) for the two forcing scenarios A2 and B2 (for numerical values, see the Appendix, Table A2). Unsurprisingly, the potential is highest in winter and lowest in summer, and it clearly increases from South to North. A significant reduction of the potential for cooling by night-time ventilation is displayed for all locations, seasons and both forcing scenarios. Differences in the response between the two scenarios were found to be comparatively small, but, as expected, scenario A2 with higher concentrations of radiatively active gases yielded generally lower $\overline{CCP}$ values than scenario B2.

Figure 5 shows the absolute and relative reduction in $\overline{CCP}$ based on forcing scenario A2 for all seasons as a function of latitude. Except in Athens, where the mean potential in summer is currently only 13 Kh per night, the absolute reduction based on forcing scenario A2 amounted to about 30–60 Kh (B2 = 20–45 Kh) (Table A2). No clear trends depending on latitude or season were found for the absolute changes (Figure 5 (left)).

Considering the relative change in $\overline{CCP}$, a clear gradient from North to South can be recognized (Figure 5 (right)). The potential for night-time cooling during the summer months (June–August) was found to decrease by about 28–51% (B2 = 21–41%) (Table A2) in Central and Northern Europe. Very high values of relative reduction in $\overline{CCP}$ of up to 94% (B2 = 86%) were detected for the two Southern European locations. It should be noted

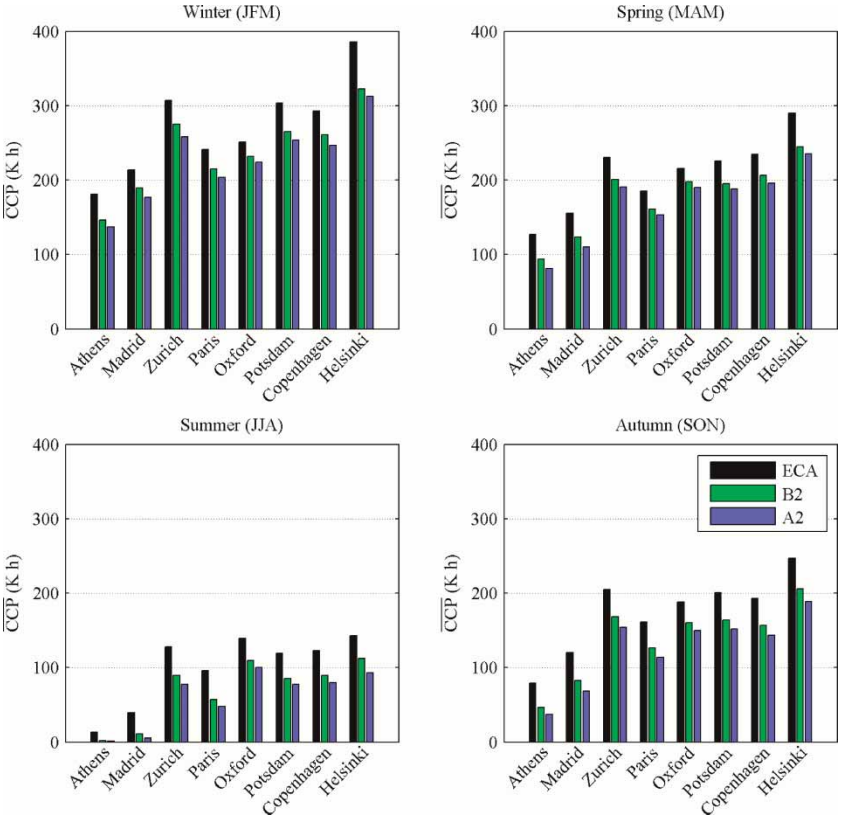

Figure 4 Estimated mean climatic cooling potential ($\overline{CCP}$) per season under current (1961–90, ECA data) and possible future (2071–2100, scenarios 'A2' and 'B2') climatic conditions at eight European locations. Future estimates present averages obtained from all selected climate scenario data sets (see 'Model-simulated temperature data') for that particular location, season and forcing scenario

that these high values are relative to the current summertime potential, which is, in fact, already insufficient for effective night-time cooling. However, in Southern Europe the potential during spring (March–May) and autumn (September–November) was also found to decrease by 29–53% (B2 = 20–42%). For all locations, the largest relative reductions occurred in summer.

Figure 6 illustrates the uncertainty of future summertime $\overline{CCP}$ estimates due to the choice of alternative

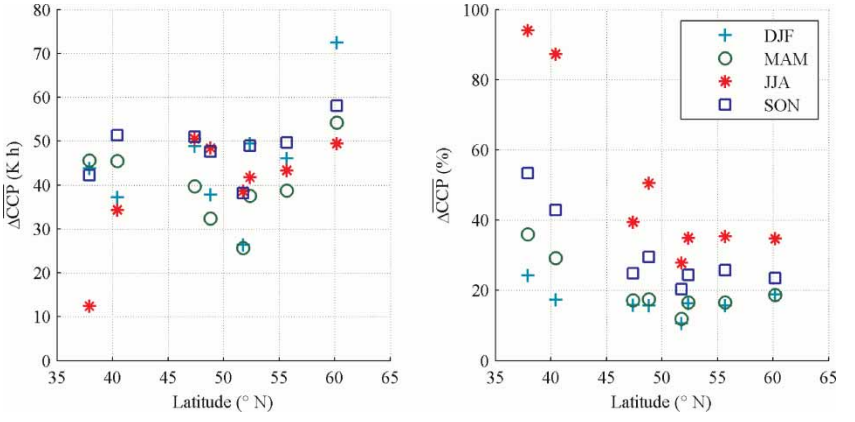

Figure 5 Absolute (left) and relative (right) changes in mean climatic cooling potential, $\Delta\overline{CCP}$ per season for 2071–2100 based on forcing scenario 'A2'. Results from eight European locations relative to the 1961–90 baseline are shown as a function of latitude. Each datum point represents the average from all selected climate scenario data sets (see 'Model-simulated temperature data') for that particular location, season and forcing scenario

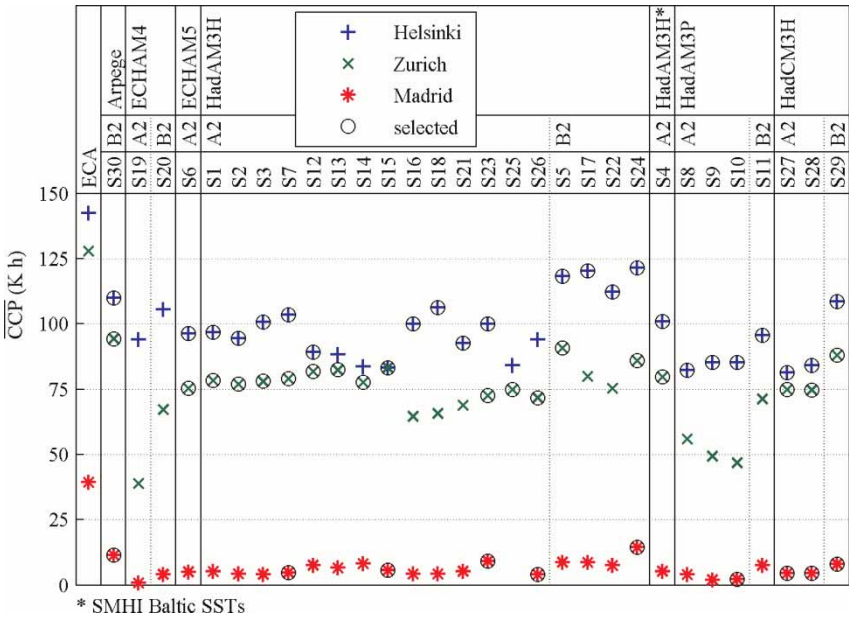

Figure 6 Mean climatic cooling potential, $\overline{CCP}$, for summer (June–August) at three selected European locations based on measured T_{min} data for 1961–90 (ECA, left column) and 30 T_{min} scenario data sets (scenarios S1–S30; see the Appendix, Table A1) for 2071–2100. All scenario data sets were constructed from regional climate model data provided by the PRUDENCE project. A2, B2: radiative forcing scenarios; Arpege, ECHAM4, ECHAM5, HadAM3H, HadAM3P and HadCM3H: global climate models used to drive the regional models; circles denote global/regional climate model configurations selected for further analysis based on an evaluation of model performance under present-day conditions (see 'Model-simulated temperature data')

forcing scenario (A2 versus B2) and GCM/RCM configuration. Results for the three locations Helsinki, Zurich and Madrid, representative for climates of Northern, Central and Southern Europe, respectively, are shown. The first column represents the $\overline{CCP}$ values based on ECA data. For ease of comparison, the results from the 30 PRUDENCE runs were sorted by forcing scenario and GCM. Figure 6 shows some interesting features in addition to what can already be discerned from Figures 4 and 5.

First, simulation runs under A2 conditions always resulted in lower $\overline{CCP}$ values than the respective B2 simulations using the same RCM/GCM configuration (compare, for example, S19 and S20). Second, differences in projected values due to the use of different RCMs under one and the same GCM simulation were often found to be of the same order as the differences due to the choice of forcing scenario. Compared with these uncertainties, the reduction in the cooling potential between current climate (1961–90) and predictions for future climate (2071–2100) was still significant. For example, at Helsinki the difference in the average $\overline{CCP}$ value from all selected (see 'Model-simulated temperature data') RCM/GCM configurations under the A2/HadAM3H boundary conditions as compared with the B2/HadAM3H boundary conditions amounted to 21 Kh. This compares with the inter-RCM range for the two boundary conditions of 23 and 9 Kh, respectively. The reduction in $\overline{CCP}$ during summer, however, amounted to 47 Kh under A2 and 29 Kh under B2 conditions. In addition, it can be seen that RCM/GCM configurations that were excluded due to poor performance under present-day conditions (data points not enclosed within a circle in Figure 6) often showed outlying $\overline{CCP}$ values (e.g. Zurich: S8, S9, S10 and S19). This also applied to other locations and seasons.

Figure 7 shows for Zurich and Madrid the percentage of nights per season under present-day and possible future conditions when the daily cooling potential $CCP_{(d)}$ exceeds a certain value. (Each curve corresponds to 1 minus the cumulative distribution function (CDF) of a $CCP_{(d)}$ data set; note also the reversal of the *x*- and *y*-axes as compared with the usual representation of CDFs). Additional charts for the other case study locations are presented in the Appendix (Figure A1).

Figure 7 suggests significant and highly variable changes in exceedance probabilities depending on location, season, and the threshold of minimum CCP necessary in a particular case. For example, at Zurich (Figure 7 (left)), under current climate conditions $CCP_{(d)}$ is higher than 80 Kh (roughly necessary to remove heat gains of 50 W/m^2; Artmann *et al.*, 2007) throughout most of the year, except for about 10% of summer nights. Under scenario A2 $CCP_{(d)}$ was found to fall below 80 Kh in more than 50% (B2 = 45%) of summer

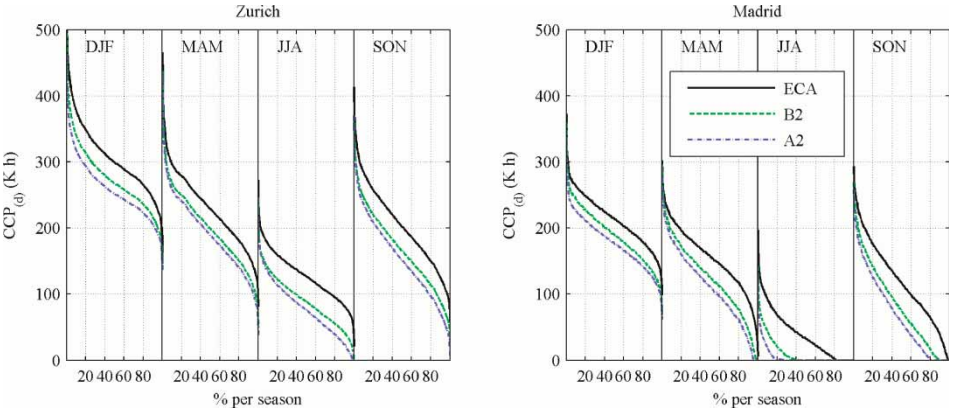

Figure 7 Percentage of nights per season under present day (ECA data, 1961–90) and possible future conditions (forcing scenarios A2 and B2, 2071–2100) during which the daily cooling potential $CCP_{(d)}$ exceeds a certain value at Zurich (left) and Madrid (right). For future conditions average percentages of nights are shown as computed from all selected climate scenario data sets (see section two) per location, season and forcing scenario

nights. Similar results were also found for Potsdam and Copenhagen. Even at the most northern location, Helsinki, under A2 conditions, 35% (B2 = 18%) of all summer nights were found to exhibit a cooling potential of less than 80 Kh per night (Figure A1).

Under present climatic conditions $CCP_{(d)}$ values at the studied locations in Southern Europe were found to be below 80 Kh throughout almost the entire summer. However, a considerable cooling potential was revealed in the transition seasons, such that the 80 Kh threshold was exceeded in 70% of all days in the year at Madrid (Athens = 57%). Under A2 conditions $CCP_{(d)}$ was found to be below 80 Kh for 48% of the year in Madrid (Figure 7 (right)) and 61% in Athens (Figure A1).

A further feature that can be discerned from Figure 7 is the changes in the variability of $CCP_{(d)}$. Significant increases in $CCP_{(d)}$ variability were typically found at the Central and Northern European locations during the summer (more stretched CDFs across the y-axis, e.g. Zurich in Figure 7). In contrast, large decreases in variability were found in cases with a low $\overline{CCP}$ under present-day conditions (e.g. Madrid in June–August and September–November) (Figure 7).

The diagram on the left in Figure 8 shows a range of the possible development of the mean climatic cooling potential, $\overline{CCP}$ during the summer (June–August) from 1990 to 2100. The lower limit indicated a rapid decrease in night cooling potential, especially after 2030. In the case of Madrid the slope of the lower limit tailed out as it approached zero. The upper limit showed a flatter slope and levelled to a constant value at the end of the 21st century.

The diagram on the right-hand side gives the time-dependent percentage of nights when $CCP_{(d)}$ exceeds

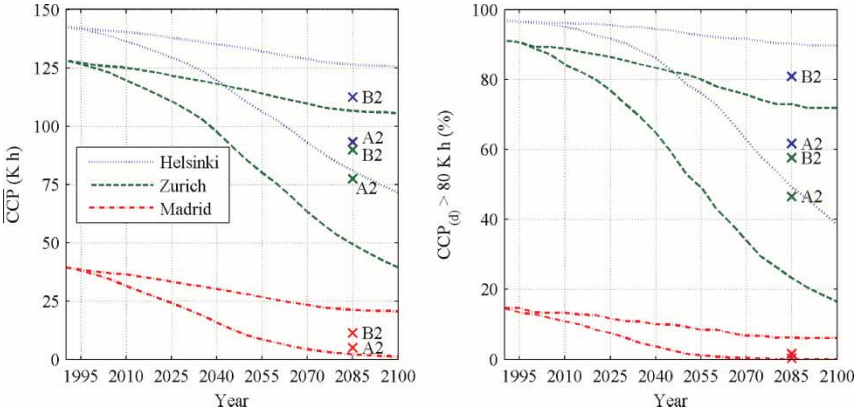

Figure 8 Time-dependent change in mean climatic cooling potential, $\overline{CCP}$ (left) and percentage of nights when $CCP_{(d)}$ exceeds 80 Kh (right) during the summer (June–August); upper and lower scenarios are based on mean global temperature scenarios (Cubash *et al.*, 2001, figure 9.14, 'several models, all SRES envelope') and mean values of selected PRUDENCE models for 'A2' and 'B2'

80 Kh. In the most extreme scenario the percentage of nights with $CCP_{(d)}$ exceeding 80 Kh in Madrid was found to decrease from 15% at present to below 1% by 2060. Until 2100 the same percentage decreased from 91% currently to 17% in Zurich and from 97 to 38% in Helsinki.

The range given by the upper and lower limits was found to be much wider than indicated by the mean values of the selected PRUDENCE models based only on forcing scenarios A2 and B2. Additionally, the position of the A2 and B2 mean values within the full range was not symmetric, and varied with location.

Discussion

The results presented here suggest that future warming will have a significant impact on the night-time ventilative cooling potential across Europe. This finding is generally in line with an earlier scenario-based analysis by Roaf *et al.* (1998), with empirical evidence for the exceptionally hot summer of 2003 (Eicker *et al.* 2006), as well as with the studies of Geros *et al.* (2005) and Kolokotroni *et al.* (2006), who concluded that in urban areas increased temperatures of a few degrees significantly lower the performance of night-time ventilation.

To the present authors' knowledge, this is the first study to provide a more in-depth assessment of possible climate change impacts on the potential for passive cooling by night-time ventilation. Unlike Roaf *et al.* (1998), who merely used a crude, threshold-based approach and coarse climate change scenarios, the present study is based upon a well-tested climatic cooling potential index (CCP; Artmann *et al.* 2007, equations 9 and 10), and explicitly accounts for temperature variations at the diurnal to century time scales. Moreover, by studying changes in probabilities at which $CCP_{(d)}$ exceeds a particular threshold value (Figures 7, 8 (right), and A1), information that is of immediate use for planning is provided.

For locations in Northern Europe, such as Copenhagen or Helsinki, the ventilative cooling potential was found to be currently sufficient throughout the entire year, whereas by 2071–2100 under conditions A2 or B2 the calculations in the present study yielded 19–48% of summer nights with a $CCP_{(d)} < 80$ Kh (Figures 8 (right) and A1). Considering that high minimum temperatures tend to coincide with generally warm days, these figures suggest an increased risk of thermal discomfort for two to six weeks per year.

Even stronger warming impacts were found for the Central European locations (Figures 7 (left), 8 and A1). For example, in Zurich the disproportionately great change in CCP during warm summer nights under scenario A2 resulted in some nights per year with zero potential, and a considerable extension of the period with less than 80 Kh (Figure 7 (left)). It seems that in decades to come summertime thermal comfort is unlikely to be achieved by night-time ventilation alone, and that eventually additional cooling systems, e.g. earth-to-air heat exchangers, will become necessary.

In Southern Europe summer cooling potential was found to be low already under present conditions (Figures 7 (right), 8 and A1), and according to the calculations in the present study it could be reduced by around 2050 to as little as 10–30 Kh, and later to zero (Figure 8). Note that by 2071–2100 for Madrid and Athens the RCMs used showed an increase in summer mean $T_{\min(d)}$ of over 5.0 and 3.6 K (data not shown) under the A2 and B2 scenarios, respectively. The additional cooling demand due to this warming in combination with the projected decrease in ventilative night cooling potential will make it particularly difficult to meet thermal comfort expectations. In order to avoid heavily increased energy consumption by mechanical cooling systems there is a great need for additional passive cooling techniques, such as radiant or evaporative cooling, and/or hybrid approaches. However, it should be noted that although cooling by night-time ventilation is expected to become increasingly ineffective during summer, it is likely to remain an attractive option in the transition seasons (Figures 7 (right) and A1). This will be even more the case if it is considered that under general warming the cooling season will tend to start earlier in spring and end later in autumn.

It should be pointed out that CCP values below about 40 Kh are increasingly sensitive to the threshold temperature ΔT_{crit} in equation (9) (Artmann *et al.*, 2007, figure 4). The value of $\Delta T_{\text{crit}} = 3$K was chosen for practical reasons. Especially in mechanically ventilated buildings night-time ventilation becomes ineffective if the temperature difference is too low. In naturally ventilated buildings a higher cooling potential might be useable by applying a lower ΔT_{crit} value. However, simulations performed during a follow-up study (Artmann *et al.*, submitted) showed that such low temperature differences can only be utilized at very high air change rates which are hardly achievable by natural forces. Therefore, the impact of ΔT_{crit} on the presented results seems small compared with other uncertainties.

A somewhat surprising result was that the estimated absolute changes in $\overline{CCP}$ were rather independent of location (Figures 4 and 5 (left)). This was first due to the linear dependence of $CCP_{(d)}$ on $T_{\min(d)}$ perturbations over a wide temperature range (equation 12 and Figure 3) in combination with the relatively small variability of the associated temperature

thresholds and coefficients (Table 2). Second, this result is also related to the fact that Figures 4 and 5 report average changes in $\overline{CCP}$ from all selected RCM simulations per location and forcing scenario. Apparently, although the climate change signal, $\Delta\overline{T}$, of individual RCMs typically shows large spatial variability (e.g. Figure 1), the use of multi-model means tended to blur inter-RCM differences, thus yielding roughly similar average responses for $\overline{CCP}$. As a consequence, relative changes in $\overline{CCP}$ were found to be largest in situations where the current $\overline{CCP}$ is smallest, i.e. at the southern-most locations and during summer (Figure 5 (right)).

The results further suggest that the uncertainty in the $\overline{CCP}$ signal due to the use of different radiative scenarios and the estimation of the associated local temperature signals by means of RCMs are of a similar magnitude (Figure 6). Similar results were also found for other locations and seasons (data not shown). This indicates that robust assessments should be based on the use of as many RCMs as possible, with the aim to cancel out errors simulated by individual RCMs.

At the same time the present analysis showed that RCMs cannot be trusted blindly. In several cases the models were found to show large biases in the simulation of present-day local $T_{\min(d)}$ (authors' analyses, cf. equations 1–4, results not shown) (also Kjellström *et al.*, 2007). Moreover, these problematic cases frequently yielded outlying $\overline{CCP}$ change values (Figure 6, e.g. for Zurich: S8, S9, S10 and S19), and using these would have introduced a strong bias in the $\overline{CCP}$ scenarios. This was also found to be the case for other seasons and locations (results not shown) and underlines the need for careful RCM evaluation and selection, as done in the present study.

The analysis at the daily time-scale revealed that future warming will have a strong impact on the cumulative distribution functions for $CCP_{(d)}$. Figure 8 illustrates the need for, and added value of, an analysis using daily data: for Helsinki and Zurich the $\overline{CCP}$ values start at a high level and show a relatively smooth, inconspicuous decrease over the first half of the 21st century (Figure 8 (left)). Yet, if exceedance probabilities for the relevant 80 Kh threshold are considered (Figure 8 (right)), practical implications would follow for the same period that could not be readily deduced from the $\overline{CCP}$ signal alone.

Also noteworthy are the great changes in the variability of $CCP_{(d)}$ – in particular during summer (Figures 7 and A1). The variability changes on the one hand reflected the generally increasing number of cases with zero potential (cf. equation 12) under a warmer climate. On the other hand, the future $CCP_{(d)}$ variability was also affected by a general increase in the variability of summertime $T_{\min(d)}$ in most RCM scenario simulations (on average 15% across all summer scenario data sets and locations; data not shown). The variability changes in the RCMs can be traced to land–atmosphere interactions that are expected to become increasingly important for the Central and Eastern European climate (Seneviratne *et al.*, 2006), and they had a significant effect on the results of the present study. For example, in Zurich it was estimated that under the A2 scenario 5% of future summer nights will have a cooling potential below 12 Kh; without changes in variability the corresponding value would have been about 21 Kh.

The increasing uncertainty range of the estimates with time (Figure 8) reflected the associated uncertainty in the evolution of the future global radiative forcing (Nakicenovic *et al.*, 2000). The 'upper' and 'lower' CCP trajectories shown in Figure 8 should by no means be considered as definitive. Rather, they present the current best estimates, given the scenarios, models and data available for this study. However, there are at least three reasons why the authors believe that the 'lower' CCP trajectories in Figure 8 might still be too optimistic.

First, the global temperature scenarios (input to equation 6) used to produce the CPP scenarios depend critically on assumptions regarding the equilibrium climate sensitivity, i.e. the equilibrium response of global mean temperature to a doubling of atmospheric CO_2 concentrations relative to the pre-industrial level. The global temperature scenarios used in this study assumed that the climate sensitivity is in the range 1.7–4.2 K (Cubasch *et al.*, 2001). More recent studies suggest, however, a 5–95% interval of 1.5–6.2 K for the equilibrium climate sensitivity (Hegerl *et al.*, 2006), or even a 95% upper limit as high as approximately 8 K (Stainforth *et al.*, 2005). The IPCC Fourth Assessment Report states a likely (>66% probability) range of 2.0–4.5 K (Meehl *et al.*, 2007), i.e. +0.3 K as compared with the bounds assumed here. Clearly, larger climate sensitivities for any given forcing scenario result in higher global temperature change rates, implying stronger local temperature signals, and consequently a more rapid decrease in cooling potential.

Second, the IPCC Fourth Assessment Report states for $\Delta\overline{T}_g$ a possible increase in the range 1.1–6.4°C in 2090–99 relative to 1980–99 (Meehl *et al.*, 2007), as opposed to the 1.3–5.5°C assumed in the present work (see 'Model-simulated temperature data'). One reason for the larger $\Delta\overline{T}_g$ range is that the new estimates incorporate the effect of carbon cycle uncertainties. However, note too that the new range was based on a set of six marker emissions scenarios that all assume that no climate change mitigation policies will be implemented. Hence, it might be argued that

the implementation of such policies would result in generally lower estimates for $\Delta\overline{T}_g$. Yet, it is unclear whether this would suffice to reduce the upper bound to below the 5.5°C assumed in the present work.

Third, this study did not account for the heat island effect that is present in many urban environments. Geros *et al.* (2005) analysed this effect for ten urban canyons situated in the extended region of Athens. Their measurements suggested a mean increase in outdoor air temperatures during the night of 0.6–2.9 K. For London, Kolokotroni *et al.* (2006) state for summer a mean heat island effect of 3.2 K. These numbers compare with the mean temperature signal for 2071–2100 in the present study that amounted to 3.8 K (2.8 K) for the A2 (B2) forcing scenario (averages across all RCMs, seasons and locations). As the heat island effect has not been considered in the present study, the true potential for night-time cooling in large urban areas could be considerably lower than stated in the given results.

Conclusions

Future climate warming will have a significant impact on the potential for cooling by night-time ventilation in Europe. Under an A2 or B2 radiative forcing scenario the authors estimate that by 2071–2100 the decrease in mean cooling potential will be in the order of 20–60 Kh, depending on season, location and forcing scenario, as compared with 80 Kh roughly necessary to remove heat gains of 50 W/m^2. Relative decreases in mean cooling potential are expected to be largest at low latitudes and for summer, i.e. cases where there is typically the highest cooling demand.

This study clearly demonstrated that any assessment of possible changes in the future ventilative night cooling potential (and probably also in any other indices related to the energy demand of buildings) is subject to large and partially irreducible uncertainties. Nevertheless, the amplitude and rate of the expected climatic changes and the longevity of buildings make planning necessary. The authors believe that it is neither possible nor desirable to establish any rigid guidelines. Instead, it is suggested that planning basics should be updated on a regular basis in order to reflect the latest developments from climate science and building physics.

The authors believe to have shown that this can be accomplished by linking high-resolution meteorological data sets, state-of-the-art climate model simulations, and applications-orientated climate scenarios with a simplified building model. More specifically, the results of the present study suggest that useful analyses of building energy balance scenarios should: (1) consider a high (e.g. daily) temporal resolution, (2) rely on as many global/regional climate models as possible, (3) account for the regionally and seasonally varying quality of these models, (4) consider changes in daily to inter-annual climate variability, in particular during summer, and (5) take into consideration the uncertainty of transient climate developments, e.g. by considering a wide range of radiative forcing scenarios and global climate sensitivities.

The decreases found in mean cooling potential have regionally varying implications. In Northern Europe (Helsinki, Copenhagen) the risk of thermal discomfort for buildings that use exclusively ventilative night cooling is expected to increase steadily up to possibly critical levels in the second half of the 21st century. In Central Europe (Zurich, Paris, London, Potsdam) extended periods with very low night cooling potential – where thermal comfort cannot be assured based on night-time ventilation only – could already become more frequent in the next few decades if a strong warming scenario became real. For Southern Europe (Athens, Madrid) the potential for ventilative night cooling will eventually become negligible during summer and will decrease to critical levels in the transition seasons.

In order to prevent a massive increase in energy consumption by mechanical cooling systems, at least three further strategies will have to be investigated: the reduction of external and internal heat gains, alternative passive cooling techniques, and the use of hybrid systems. The latter approach might be particularly attractive for Central Europe during summer, where a substantial potential for night-time cooling is likely to remain throughout the 21st century. In Southern Europe the hybrid approach could be attractive at least during the transition seasons due to the expected prolongation of the cooling season in combination with a generally increased cooling demand throughout the year.

In any case, in view of the need to abate global warming and to reduce dependency on fossil fuels, the authors believe that building design should be based on energy-efficient passive cooling techniques whenever possible.

Acknowledgements

This work was partially funded by the Hybrid Ventilation Centre, Department of Civil Engineering, Aalborg University, and the Swiss Federal Office of Energy (Project No. 101'308). The project was also supported by the private sector (WindowMaster, Belimo, SZFF). The authors acknowledge with thanks all financial support. Data were provided through the PRUDENCE data archive, funded by the European Union through Contract No. EVK2-CT2001-00132.

References

Allard, F. (1998) *Natural Ventilation in Buildings*, James & James, London.

Artmann, N., Manz, H. and Heiselberg, P. (2007) Climatic potential for passive cooling of buildings by night-time ventilation in Europe. *Applied Energy*, **84**, 187–201.

Artmann, N., Manz, H. and Heiselberg, P. (submitted) Parameter study on performance of building cooling by night-time ventilation. *Renewable Energy*.

CEN (1998) *Ventilation for Buildings: Design Criteria for the Indoor Environment*. CR 1752, CEN, Brussels.

Chandra, S. (1989) Ventilative cooling, in J. Cook (ed.): *Passive Cooling*, MIT Press, Cambridge, MA, p. 70.

Chartered Institution of Building Services Engineers (CIBSE) (2005) *TM36, Climate Change and the Indoor Environment: Impacts and Adaptation*. Technical Memorandum No. 36, CIBSE, London.

Christensen, J.H., Carter, T.R. and Giorgi, F. (2002) PRUDENCE employs new methods to assess European climate change. *EOS, Transactions of the American Geophysical Union*, **83**(13), 147.

Christensen, J.H., Carter, T.R., Rummukainen M. and Amanatidis, G. (2007) Evaluating the performance and utility of climate models: the PRUDENCE project. *Climatic Change*, **81**(Suppl. 1), 1–6.

Christenson, M., Manz, H. and Gyalistras, D. (2005) Climate warming impact on degree-days and building energy demand in Switzerland. *Energy Conversion and Management*, **47**, 671–686.

Cubasch, U., Meehl, G.A., Boer, G.J., Stouffer, R.J., Dix, M., Noda, A., Senior, C.A., Raper, S., Yap, K.S. *et al.* (2001) Projections of future climate change, in J.T. Houghton, Y. Ding, D.J. Griggs, M. Noguer, P.J. van der Linden, X.D. Dai, K. Maskell and C.A. Johnson (eds): *Climate Change 2001: The Scientific Basis*. Contribution of Working Group I to the Third Assessment Report of the Intergovernmental Panel on Climate Change (IPCC), Cambridge University Press, Cambridge, pp. 525–582 (available at: http://www.grida.no/climate/ipcc_tar/wg1/338.htm).

Eicker, U., Huber, M., Seeberger, P. and Vorschulze, C. (2006) Limits and potentials of office building climatisation with ambient air. *Energy and Buildings*, **38**, 574–581.

Engineering and Physical Sciences Research Council (EPSRC) (2003) *Building Knowledge for a Changing Climate – The Impacts of Climate Change on the Built Environment*, UK Climate Impacts Programme, Oxford.

Frank, T. (2005) Climate change impacts on building heating and cooling energy demand in Switzerland. *Energy and Buildings*, **37**, 1175–1185.

Geros, V., Santamouris, M., Karatasou, S., Tsangrassoulis, A. and Papanikolaou, N. (2005) On the cooling potential of night ventilation techniques in the urban environment. *Energy and Buildings*, **37**, 243–257.

Giorgi, F., Hewitson, B., Christensen, J., Hulme, M., Von Storch, H., Whetton, P., Jones, R., Mearns, L., Fu, C. *et al.* (2001) Regional climate information – evaluation and projections, in J.T. Houghton, Y. Ding, D.J. Griggs, M. Noguer, P.J. van der Linden, X.D. Dai, K. Maskell and C.A. Johnson (eds): *Climate Change 2001: The Scientific Basis*. Contribution of Working Group I to the Third Assessment Report of the Intergovernmental Panel on Climate Change (IPCC), Cambridge University Press, Cambridge, pp. 583–638.

Gyalistras, D., Schär, C., Davies, H.C. and Wanner, H. (1998) Future Alpine climate, in P. Cebon, U. Dahinden, H.C. Davies, D. Imboden, C.G. Jäger (eds): *Views from the Alps: Regional Perspectives on Climate Change*, MIT Press, Boston, pp. 171–223.

Hegerl, G.C., Crowley, T.J., Hyde, W.T. and Frame, D.J. (2006) Constraints on climate sensitivity from temperature reconstructions of the past seven centuries. *Nature*, **440**, 1029–1032.

Intergovernmental Panel on Climate Change (IPCC) (2006) (available at: http://www.ipcc.ch) (accessed May 2006).

International Standards Organization (ISO) (1994) *Moderate Thermal Environments – Determination of the PMV and PPD Indices and Specification of the Conditions for Thermal Comfort*. ISO 7730, ISO, Geneva.

Kjellström, E., Bärring, L., Jacob, D., Jones, R.J., Lenderink, G. and Schär, C. (2007) Modelling daily temperature extremes: recent climate and future changes over Europe, *Climatic Change*, **81**, 249–265.

Klein Tank, A.M.G. *et al.* (2002) Daily data set of 20th-century surface air temperature and precipitation series for the European Climate Assessment, International Journal of Climatology, **22**, 1441–1453 (data and metadata available at: http://eca.knmi.nl).

Kolokotroni, M., Giannitsaris, I. and Watkins, R. (2006) The effect of the London urban heat island on building cooling demand and night ventilation strategies. *Solar Energy*, **80**, 383–392.

Manz, H. (2004) Total solar energy transmittance of glass double façades with free convection, *Energy and Buildings*, **36**, 127–136.

Manz, H. and Frank, T. (2005) Thermal simulation of buildings with double-skin façades, *Energy and Buildings*, **37**, 1114–1121.

Mearns, L.O., Hulme, M., Carter, T.R., Leemans, R., Lal, M., Whetton, P. *et al.* (2001) Climate scenario development, in J.T. Houghton, Y. Ding, D.J. Griggs, M. Noguer, P.J. van der Linden, X.D. Dai, K. Maskell and C.A. Johnson (eds): *Climate Change 2001: The Scientific Basis*. Contribution of Working Group I to the Third Assessment Report of the Intergovernmental Panel on Climate Change (IPCC), Cambridge University Press, Cambridge, pp. 739–768.

Meehl, G.A., Stocker, T.F., Collins, W.D., Friedlingstein, P., Gaye, A.T., Gregory, J.M., Kitoh, A., Knutti, R., Murphy, J.M., Noda, A., Raper, S.C.B., Watterson, I.G., Weaver, A.J. and Zhao, Z.-C. (2007) Global climate projections, in S. Solomon, D. Qin, M. Manning, Z. Chen, M. Marquis, K.B. Averyt, M. Tignor and H.L. Miller (eds): *Climate Change 2007: The Physical Science Basis*. Contribution of Working Group I to the Fourth Assessment Report of the Intergovernmental Panel on Climate Change, Cambridge University Press, Cambridge, pp. 747–845.

Meteonorm (2005) *Global Meteorological Database for Engineers, Planners and Education*, Version 5.1 (available at: http://www.meteonorm.com).

Mitchell, T.D. (2003) Pattern scaling: an examination of the accuracy of the technique for describing future climates. *Climatic Change*, **60**(3), 217–242.

Nakicenovic, N., Alcamo, J., Davis, G., De Vries, B., Fenhann, J., Gaffin, S., Gregory, K., Grübler, A., Jung, T.Y., Kram, T., La Rovere, E.L., Michaelis, L., Mori, S., Morita, T., Pepper, W., Pitcher, H., Price, L., Raihi, K., Roehrl, A., Rogner, H.-H., Sankovski, A., Schlesinger, M., Shukla, P., Smith, S., Swart, R., Van Rooijen, S., Victor, N. and Dadi, Z. (2000) *IPCC Special Report on Emissions Scenarios*, Cambridge University Press, Cambridge.

Olesen, B.W. and Parsons, K.C. (2002) Introduction to thermal comfort standards and to the proposed new version of EN ISO 7730. *Energy and Buildings*, **34**, 537–548.

PRUDENCE (2005) *Prediction of Regional scenarios and Uncertainties for Defining European Climate Change Risks and Effects*. Final Report 2005 (available at: http://prudence.dmi.dk).

PRUDENCE (2006) (available at: http://prudence.dmi.dk) (accessed April 2006).

Roaf, S., Haves, P. and Orr, J. (1998) Climate change and passive cooling in Europe, in *Proceedings of 'Environmentally Friendly Cities'*, PLEA '98 (Passive and Low Energy Architecture) Conference, Lisbon, Portugal, June 1998, pp. 463–466.

Santamouris, M. and Asimakopoulos, D. (1996) *Passive Cooling of Buildings*. London, UK: James & James.

Schaer, C., Vidale, P.L., Luethi, D., Frei, C., Haeberli, C., Liniger, M.A. and Appenzeller, C. (2004) The role of increasing temperature variability in European summer heatwaves. *Nature*, **427**, 332–336.

Seneviratne, S.I., Lüthi, D., Litschi, M. and Schär, Ch. (2006) Land–atmosphere coupling and climate change in Europe. *Nature*, **443**, 205–209.

Stainforth, D.A., Aina, T., Christensen, C., Collins, M., Faull, N., Frame, D.J., Kettleborough, J.A., Knight, S., Martin, A., Murphy, J.M., Piani, C., Sexton, D., Smith, L.A., Spicer, R.A., Thorpe, A.J. and Allen, M.R. (2005). Uncertainty in predictions of the climate response to rising levels of greenhouse gases. *Nature*, **433**, 403–406.

Trenberth, K.E., Jones, P.D., Ambenje, P. Bojariu, R., Easterling, D., Klein Tank, A., Parker, D., Rahimzadeh, F., Renwick, J.A., Rusticucci, M., Soden, B. and Zhai, P. (2007) Observations: surface and atmospheric climate change, in S. Solomon, D. Qin, M. Manning, Z. Chen, M. Marquis, K.B. Averyt, M. Tignor and H.L. Miller (eds): *Climate Change 2007: The Physical Science Basis*. Contribution of Working Group I to the Fourth Assessment Report of the Intergovernmental Panel on Climate Change, Cambridge University Press, Cambridge, pp. 235–336.

Appendix

Table A1 PRUDENCE scenario and corresponding control data sets

Institute	Model	Scenario					Control	
		Number	Driving data	Forcing	$\Delta\bar{T}_{GCM}$	Acronym	Number	Acronym
DMI	HIRHAM	S1	HadAM3H	A2	3.2	HS1	C1	HC1
DMI	HIRHAM	S2	HadAM3H	A2	3.2	HS2	C2	HC2
DMI	HIRHAM	S3	HadAM3H	A2	3.2	HS3	C3	HC3
DMI	HIRHAM	S4	HadAM3H (SMHI Baltic SSTs)	A2	–	HS4	C1	HC1
DMI	HIRHAM	S5	HadAM3H	B2	2.3	HB1	C1	HC1
DMI	HIRHAM	S6	ECHAM5	A2	–	ECS	C4	ECC
DMI	HIRHAM h. r.	S7	HadAM3H	A2	3.2	S25	C5	F25
HC	HadRM3P	S8	HadAM3P	A2	–	Adhfa	C6	adeha
HC	HadRM3P	S9	HadAM3P	A2	–	Adhfe	C7	adehb
HC	HadRM3P	S10	HadAM3P	A2	–	Adhff	C8	adehc
HC	HadRM3P	S11	HadAM3P	B2	–	Adhfd	C6	adeha
ETH	CHRM	S12	HadAM3H	A2	3.2	HC_A2	C9	HC_CTL
GKSS	CLM	S13	HadAM3H	A2	3.2	SA2	C10	CTL
GKSS	CLM impr.	S14	HadAM3H	A2	3.2	SA2sn	C11	CTLsn
MPI	REMO	S15	HadAM3H	A2	3.2	3006	C12	3003
SMHI	RCAO	S16	HadAM3H	A2	3.2	HCA2	C13	HCCTL
SMHI	RCAO	S17	HadAM3H	B2	2.3	HCB2	C13	HCCTL
SMHI	RCAO h. r.	S18	HadAM3H	A2	3.2	HCA2_22	C14	HCCTL_22
SMHI	RCAO	S19	ECHAM4/OPYC	A2	3.4	MPIA2	C15	MPICTL
SMHI	RCAO	S20	ECHAM4/OPYC	B2	2.6	MPIB2	C15	MPICTL
UCM	PROMES	S21	HadAM3H	A2	3.2	a2	C16	control
UCM	PROMES	S22	HadAM3H	B2	2.3	b2	C16	control
ICTP	RegCM	S23	HadAM3H	A2	3.2	A2	C17	ref
ICTP	RegCM	S24	HadAM3H	B2	2.3	B2	C17	ref
met.no	HIRHAM	S25	HadAM3H	A2	3.2	HADCN	C18	HADCN
KNMI	RACMO	S26	HadAM3H	A2	3.2	HA2	C19	HC1
CNRM	Arpege	S27	HadCM3H	A2	–	DE6	C20	DA9
CNRM	Arpege	S28	HadCM3H	A2	–	DE7	C20	DA9
CNRM	Arpege	S29	HadCM3H	B2	–	DE5	C20	DA9
CNRM	Arpege	S30	Arpege/OPA	B2	–	DC9	C20	DA9

Table A2 Mean climatic cooling potential per season (Kh/night) under current (1961–90) and future (2071–2100 A2 and B2) climatic conditions, absolute and relative reduction at different locations

Location	Season	1961–90	2071–2100 A2			2071–2100 B2		
		CCP (Kh)	CCP (Kh)	ΔCCP (Kh)	ΔCCP (%)	CCP (Kh)	ΔCCP (Kh)	ΔCCP (%)
Helsinki	December–February	385	312	73	19.0	321	64	16.7
	March–May	290	236	54	18.5	245	45	15.6
	June–August	143	96	47	32.8	114	29	20.3
	September–November	247	189	58	23.5	206	41	16.7
Copenhagen	December–February	293	246	47	16.1	255	38	12.9
	March–May	234	195	39	16.8	204	30	12.8
	June–August	123	81	42	34.3	90	33	26.8
	September–November	193	144	49	25.2	157	36	18.6
Potsdam	December–February	304	255	49	16.0	265	38	12.6
	March–May	225	187	38	16.9	196	29	13.0
	June–August	119	77	42	35.5	87	33	27.5
	September–November	201	153	48	23.9	164	37	18.4
Oxford	December–February	251	224	26	10.6	232	18	7.4
	March–May	216	189	27	12.4	196	20	9.3
	June–August	139	102	37	26.8	111	28	19.8
	September–November	188	150	38	20.1	161	27	14.2
Paris	December–February	241	203	38	15.8	216	25	10.5
	March–May	185	154	32	17.2	161	24	13.0
	June–August	96	48	48	49.7	52	44	45.5
	September–November	161	115	46	28.6	126	35	21.8
Zurich	December–February	307	260	48	15.5	280	27	8.9
	March–May	230	193	37	16.3	208	22	9.7
	June–August	128	78	50	39.2	88	40	31.0
	September–November	205	154	51	24.8	167	38	18.7
Madrid	December–February	214	176	38	17.6	190	24	11.3
	March–May	156	110	46	29.4	124	31	20.2
	June–August	39	5	34	86.5	12	28	70.6
	September–November	120	70	49	41.3	83	36	30.4
Athens	December–February	181	137	44	24.5	148	32	18.0
	March–May	127	82	45	35.5	94	33	25.9
	June–August	13	1	12	94.2	2	11	86.4
	September–November	79	36	43	54.5	46	33	42.2

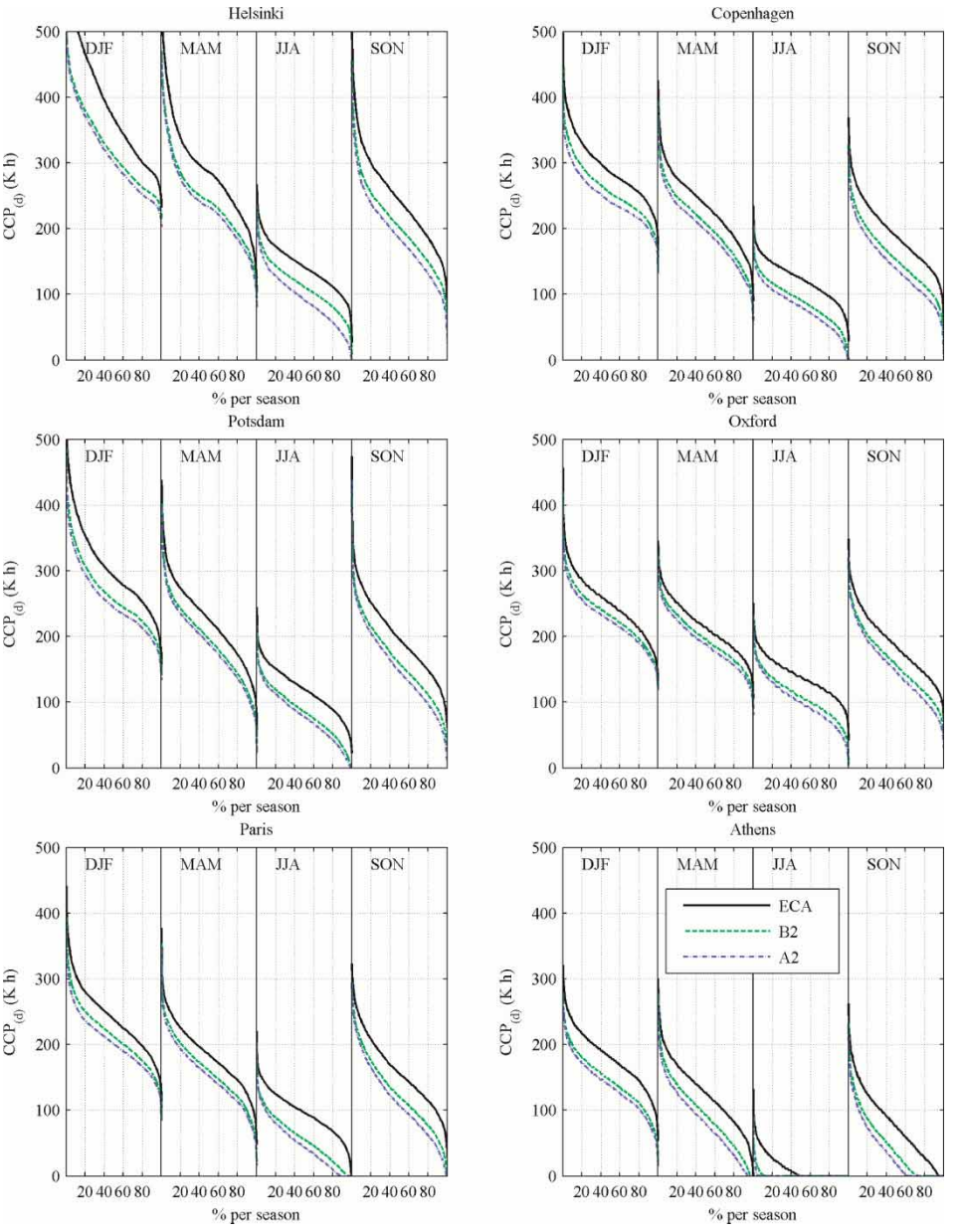

Figure A1 Seasonal cumulative distributions of CCP at different locations under current climatic conditions (ECA data) and projections based on forcing scenarios A2 and B2